AGU PUBLICATIONS

JGR

Journal of Geophysical Research: Atmospheres

RESEARCH ARTICLE
10.1002/2015JD023419

Key Points:
- First deployment of an aerosol mass spectrometer (AMS) in India
- Foggy-period organic aerosols were more oxidized during than nonfoggy period
- Biomass burning contributed a large fraction of organic aerosols

Supporting Information:
- Text S1, Table S1, and Figures S1–S13
- Figure S1
- Figure S2
- Figure S3
- Figure S4a
- Figure S4b
- Figure S5
- Figure S6
- Figure S7
- Figure S8a
- Figure S8b
- Figure S9
- Figure S10
- Figure S11
- Figure S12
- Figure S13

Correspondence to:
T. Gupta and S. N. Tripathi,
tarun@iitk.ac.in;
snt@iitk.ac.in

Citation:
Chakraborty, A., D. Bhattu, T. Gupta, S. N. Tripathi, and M. R. Canagaratna (2015), Real-time measurements of ambient aerosols in a polluted Indian city: Sources, characteristics, and processing of organic aerosols during foggy and nonfoggy periods, *J. Geophys. Res. Atmos.*, *120*, 9006–9019, doi:10.1002/2015JD023419.

Received 23 MAR 2015
Accepted 29 JUL 2015
Accepted article online 1 AUG 2015
Published online 9 SEP 2015

Real-time measurements of ambient aerosols in a polluted Indian city: Sources, characteristics, and processing of organic aerosols during foggy and nonfoggy periods

Abhishek Chakraborty[1], Deepika Bhattu[1], Tarun Gupta[1,2], Sachchida N. Tripathi[1,2], and Manjula R. Canagaratna[3]

[1]Department of Civil Engineering, Indian Institute of Technology Kanpur, Kanpur, India, [2]Center for Environmental Science and Engineering, Indian Institute of Technology Kanpur, Kanpur, India, [3]Aerodyne Research, Billerica, Massachusetts, USA

Abstract A detailed time-resolved chemical characterization of ambient nonrefractory submicron aerosols ($NR\text{-}PM_1$) was conducted for the first time in India. The measurements were performed during the winter (November 2011 to January 2012) in a heavily polluted city of Kanpur, which is situated in the Indo-Gangetic Plain. Real-time measurements provided new insights into the sources and evolution of organic aerosols (OA) that could not be obtained using previously deployed filter-based measurements at this site. The average $NR\text{-}PM_1$ loading was very high ($>100\ \mu g/m^3$) throughout the study, with OA contributing approximately 70% of the total aerosol mass. Source apportionment of the OA using positive matrix factorization revealed large contributions from fresh and aged biomass burning OA throughout the entire study period. A back trajectory analysis showed that the polluted air masses were affected by local sources and distant source regions where the burning of paddy residues occurs annually during winter. Several fog episodes were encountered during the study, and the OA composition varied between foggy and nonfoggy periods, with higher oxygen to carbon (O/C) ratios during the foggy periods. The evolution of OA and their elemental ratios (O:C and H:C) were investigated for the possible effects of fog processing.

1. Introduction

Submicron ambient aerosols can directly and indirectly affect radiative climate forcing and are harmful to human health [*Jacobson et al.*, 2000; *Seinfeld and Pankow*, 2003; *Jimenez et al.*, 2009]. Most Indian cities have bad air quality, and several studies have reported very high aerosol loadings in all major cities across the country [*Venkataraman et al.*, 2002; *Gurjar et al.*, 2004; *Gupta et al.*, 2006; *Sarkar et al.*, 2010; *Joseph et al.*, 2012]. Kanpur is one of the major industrial hubs in India that has very poor air quality in terms of particulate matter (PM) pollution [*National Ambient Air Quality Standards* (*NAAQS*), 2012]. Several field studies [*Kaul et al.*, 2011, 2012; *Ram and Sarin*, 2011; *Gupta and Mandariya*, 2013; *Singh et al.*, 2014] have been carried out in Kanpur during winter over the past few years, and all have reported high-average PM_1 loadings varying from 100 to 530 $\mu g/m^3$. Although these studies have been useful, they mostly involved 8 h filter-based offline techniques that have failed to capture the organic aerosol evolution (changes in organic aerosols (OA) composition and properties via aging, mixing, volatilization, etc., [*Heald et al.*, 2010]) that occurs over shorter timescales. In recent years, advances in mass spectrometry and the development of the aerodyne aerosol mass spectrometer [*DeCarlo et al.*, 2006; *Canagaratna et al.*, 2007] have offered a unique opportunity for gaining insight into the evolution of OA in real time [*Hallquist et al.*, 2009; *Heald et al.*, 2010]. Many field studies have been conducted worldwide using aerosol mass spectrometer (AMS); however, the characterization and evolution of OA in South Asia, one of the most populous regions in the world, have been severely underreported. Thus, the objective of this study was to explore, for the first time, the real-time variations of different aerosol constituents while focusing on the composition and sources of OA and the effects of fog at Kanpur, a polluted urban location in India. During winter, the meteorology of Kanpur favors the accumulation of pollutants due to low wind speeds and low boundary heights. Every winter, Kanpur witnesses several short (3 h) to long (18 h) fog episodes that severely disrupt normal daily life. Fog episodes are also linked to the enhanced production of secondary organic aerosols (SOA) via aqueous processing at this location [*Kaul et al.*, 2011] and elsewhere [*Osto et al.*, 2009; *Li et al.*, 2013].

During winter, local biomass burning is a major contributor [*Behera and Sharma*, 2010b; *Kaul et al*., 2011] to aerosol loadings at this location, in addition to other sources, such as vehicular/industrial emissions and the secondary aerosol production. Biomass burning organic aerosols (BBOA) are considered major contributors to the global OA budget, both in the form of primary OA (POA) [*Bond et al*., 2004; *De Gouw and Jimenez*, 2009] and SOA [*Grieshop et al*., 2009a, 2009b]. Generally, BBOA can have very different properties, depending on the fuel type, the burning conditions, and other parameters [*Saarikoski et al*., 2008; *Ortega et al*., 2013], and they have been linked to enhanced haze formation and visibility degradation [*Ryu et al*., 2007; *Cheng et al*., 2014]. AMS inlet cutoff size, however, does not allow direct sampling of fog droplets, so in this manuscript, we mostly investigated the differences between the mass concentrations and chemical compositions of the unactivated and unscavenged fraction of ambient NR (nonrefractory) PM_1 observed during the foggy and nonfoggy periods of the study period.

2. Materials and Methods

2.1. Measurement Site and Study Period

The real-time ambient aerosol measurements were carried out at the Indian Institute of Technology (IIT) Kanpur in India (26.5°N, 80.3°E, and 142 m above mean sea level). Kanpur is located in the center of the Indo-Gangetic Plain and is a large urban environment with a population of ≃4.5 million [*Government of India*, 2011] and seriously bad air quality [*NAAQS*, 2012]. IIT Kanpur is located away from the city center but within the city boundaries. The entire study was divided into two separate periods; the first period was from 2 to 18 November 2012 and characterized by a moderate relative humidity (RH) and temperature with no fog/haze events, so the entire period was designated as nonfoggy period (P1). The second period was from 20 December 2012 to 10 January 2013 and characterized by very low temperatures, high RH, and several (10) fog events; hence, P2 was designated as foggy period. We further divided the second period into foggy periods (P2_FP) and nonfoggy periods (P2_NFP). P2_FP included the time periods of fog (mostly from late night to early morning), and P2_NFP was composed of the remaining periods (during which the nights were mostly hazy) in P2. By World Meteorological Organization definition, fog indicates an atmospheric condition with visibility < 1 km and RH close to 100% and hazy conditions associated with 1 km $<$ visibility < 5 km with RH ~80% [*Quan et al*., 2011]. In the absence of visibility measurements, we defined the beginning of a fog event as having a LWC (liquid water content) ≥ 80 mg/m^3 [*Gilardoni et al*., 2014] for ≥ 15 min and marked the end of a fog event when LWC < 80 mg/m^3 for > 15 min. (Figure S1 in the supporting information).

2.2. Instrumentation

A HR-ToF-AMS (high-resolution time-of-flight aerosol mass spectrometer) [*DeCarlo et al*., 2006; *Canagaratna et al*., 2007] was deployed for the first time in India, along with supporting instruments, including a scanning mobility particle sizer (SMPS, TSI Inc.) and a cloud combination probe (CCP, Droplet Measurement Technologies, to measure the LWC). The CCP was positioned at the rooftop of the laboratory building (at a height of 10 m above ground), and other instruments were housed inside the laboratory. Particle transmission efficiency of AMS is close to 100% from 100 to 700 nm particle size range [*Liu et al*., 2007], which is much lower than a typical fog droplet size, so during a fog event AMS can only measure interstitial aerosols, unactivated droplets [*Frank et al*., 1998] and residual aerosols left behind after fog evaporates. The CCP is primarily designed for aircraft sampling; however, in this study, the inlet was modified using an aspirator [*Singh*, 2011]. The CCP can measure different parameters and also includes a cloud imaging probe, but in this study only the CDP (cloud droplet probe) was used to measure LWC. The CDP uses a diode laser to count and size individual water droplets. The CCP measures droplet size distributions from 3 to 50 μm divided into 30 bins [*Lance et al*., 2010]; the bins are 1 μm wide from 3 to 14 μm, after which they become 2 μm wide. The AMS was operated in both high-sensitivity V and high-resolution W mode with a 1 min sampling time for each mode. The AMS was calibrated for inlet flow, ionization efficiency (IE), and particle sizing following standard protocols [*Jayne et al*., 2000; *Jimenez et al*., 2003; *Drewnick et al*., 2005]. Regular IE calibrations were performed before, during, and after the experiment. Furthermore, High efficiency particle arrestance/zero particle filter measurements were made at intervals of 2–3 days and during IE calibrations to assess the presence of gaseous interference in the mass spectra. The average relative ionization efficiencies of ammonium were 4.6 and 4.8 for the first and second periods, respectively, based on the IE calibrations, and were used to calculate the

Table 1. Campaign Average (± Standard Deviation) Meteorological Parameters

Period	Day	Night
P1	RH (%) = 65.8 (±3), T = 25°C (±4)	RH (%) = 70 (±5), T = 20°C (±3)
P2_NFP	RH (%) = 72 (±3), T = 22°C (±4), WS = 1.42 m/s (±0.7)	RH (%) = 78 (±3), T = 14°C (±3), WS = 1.21 m/s (±0.5)
P2_FP	RH (%) = 94.6 (±4), T = 5.4°C (±0.8), LWC = 197 (±53) mg/m^3, WS = 0.66 m/s (±0.4)	

NH_4^+(measured)/NH_4^+(predicted) ratio or aerosol neutralization ratio (ANR). The calculated ANR agrees with previous filter-based measurements obtained at the same location [*Gupta and Mandariya*, 2013].

2.3. Data Analysis

The AMS unit mass resolution (UMR) data were analyzed using the data analysis toolkit SQUIRREL (v1.51H), and the AMS high-resolution (HR) data were analyzed using PIKA (v1.10H) in IgorPro. HR fitting was carried out in both V and W mode up to *m/z* 150. The V mode data were used to calculate the mass concentrations of the different species and in PMF, while W mode data were used to determine the elemental ratios, although V and W mode elemental ratios were within 2–5% of each other. For both the periods, all of the data points were well within the f44 versus the f43 space (see Figure S3 in the supporting information) typical for the ambient measurements [*Ng et al.*, 2011]. Details regarding data processing procedures can be found elsewhere [*Allan*, 2003; *Aiken et al.*, 2007, 2008]. PMF analysis was carried out using the PMF evaluation tool [*Paatero and Tapper*, 1994; *Ulbrich et al.*, 2009]. The quantitative accuracy of the AMS depends on the choice of the CE (collection efficiency) value. We used *Middlebrook et al.*'s [2012] formulation, which incorporates the effects of acidity, inlet RH, and chemical composition of sampled aerosols to calculate the CE value for both the periods; from that a calculated CE of 0.5 was used to determine the concentrations of the different species. This value has been used in numerous field studies worldwide [*Canagaratna et al.*, 2007; *Middlebrook et al.*, 2012]. The choice of this CE value (0.5) was also justified by good agreement between AMS and SMPS mass concentration(s) (Figure S2). Other uncertainties related to AMS measurements are well documented in the literature [*Allan*, 2003; *Aiken et al.*, 2007; *Bahreini et al.*, 2009]. The standard fragmentation table was modified at m/z values of 15, 29, and 44, based on HEPA filter measurements. A back trajectory analysis was performed for both the periods, and the air masses mostly arrived from the north-northwest, which is the predominant wind direction during this season at this location [*Behera and Sharma*, 2010b; *Patidar et al.*, 2012].

3. Results and Discussions

3.1. Overall Meteorological Conditions, Aerosol Composition, Diurnal Variation, and Acidity

The average RH (%), T (°C), WS (wind speed) (only for P2, data are not available for P1), and LWC (shown only for foggy period) for both the periods are shown in Table 1.

Fog usually forms when air becomes saturated with water vapor (RH ~ 100%); however, several studies at polluted locations like Kanpur [*Kaul et al.*, 2011; *Gupta and Mandariya*, 2013; *Singh et al.*, 2014] and Hong Kong [*Li et al.*, 2013; *Meng et al.*, 2014] have reported fog formation at a relatively lower RH values. *Deng et al.* [2008] have shown that at higher RH, currently available RH measuring instruments have a negative bias of at least 5%. This bias in current RH measurements at higher RH may explain the observation of fog at apparently subsaturated conditions.

The overall NR-PM_1 composition, as calculated from a HR analysis, was dominated by organics (~70% of total mass) (Figure 1a). The aerosol loading was higher during P2, with an overall value of 139 ± 44 μg/m^3 (mean ± standard deviation, this convention will be followed throughout the paper) and a value of 152 ± 35 μg/m^3 at night; the corresponding overall aerosol loading and nighttime loading values during P1 were 100 ± 37 μg/m^3 and 110 ± 34 μg/m^3, respectively. During the P2_FP nighttime, when actual fog events were observed, the loading was slightly lower (132 ± 30 μg/m^3) than for P2_NFP nighttime (162 ± 38 μg/m^3) when fog events were not observed. Some of this difference may be attributed to particle scavenging and removal by fog.

The aforementioned values are well within the range of previously reported PM_1 values (100–530 μg/m^3) from filter studies and AMS measurements at the same location [*Tare et al.*, 2006; *Gupta and Mandariya*, 2013; *Singh et al.*, 2014; *Bhattu and Tripathi*, 2015]. The extremely high NR-PM_1 loadings and the overwhelming

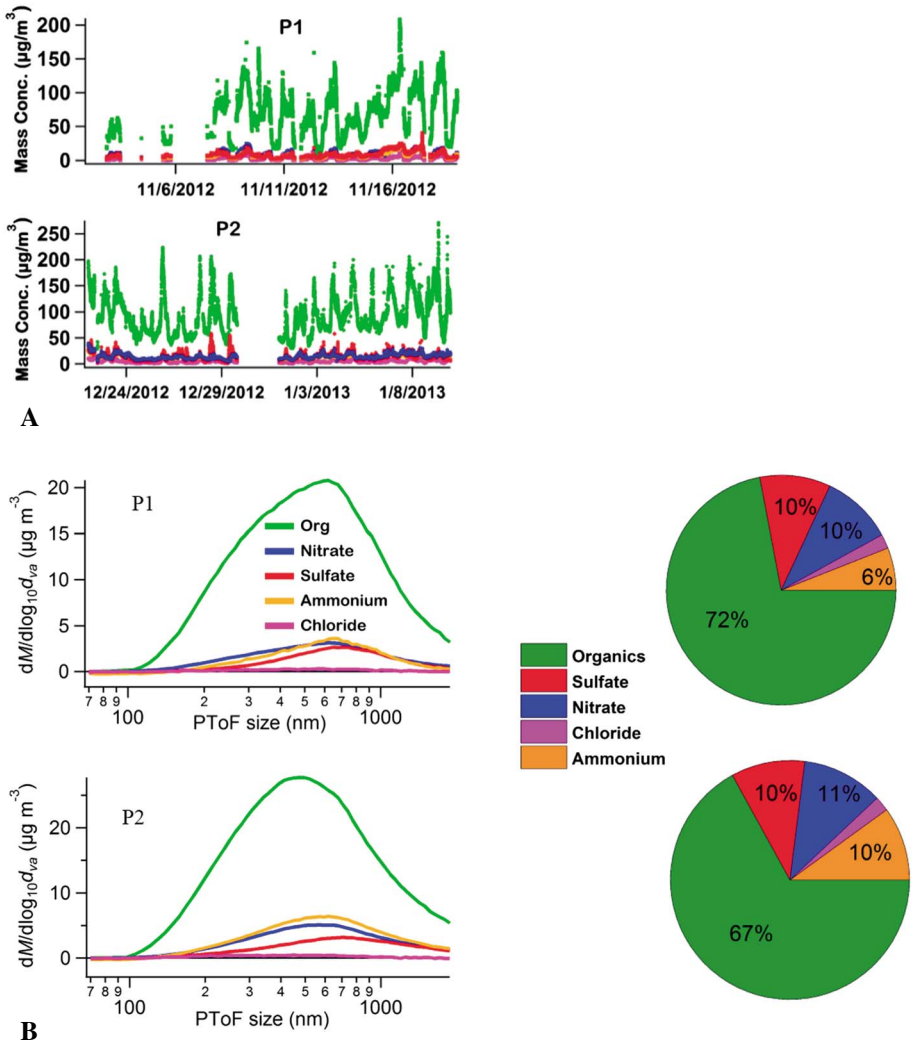

Figure 1. (a) Time series for NR-PM_1 aerosol species. Every species mass concentration(s) was increased from P1 to P2. (b) Overall composition and size distribution of NR PM_1 during P2 and P1.

dominance of the OA were different from previously reported AMS results for other winter field studies carried out elsewhere [*Zhang et al.*, 2007b], including studies that were performed in China (as shown in Table S1 in the supporting information). Such extremely high NR-PM_1 levels were only reported during extreme haze events in China in 2013 [*Zhang et al.*, 2014], which provides a sense of the extent of pollution at the current sampling location. The overall size distribution of all of the aerosol species during both the periods was broad (Figure 1b), with modes between 400 and 700 nm (for the vacuum aerodynamic diameter (dva)), indicating the significant presence of aged regional aerosols [*Alfarra et al.*, 2004; *Zhang et al.*, 2005]. The size distribution of the organics was broader than that of the other species and extended to smaller sizes, as reported in another AMS study from this location [*Bhattu and Tripathi*, 2015]. Thus, organic aerosols were more dominant with respect to their total mass over the low size ranges relative to the other size ranges. The dominance of the OA at smaller sizes (Figure S4) was reasonable considering the fresh emissions of carbonaceous particles from vehicles in urban environments, which typically have smaller mass-weighted size distribution [*Canagaratna et al.*, 2004; *Huang et al.*, 2011]. The mode of the organic size distribution was lower for P2 than for P1, which could be attributed to large contributions from fresh and aged primary OA (discussed in section 3.4.1) that usually have a smaller mode [*Huang et al.*, 2011] and/or the scavenging of larger particles by fog.

The diurnal variations of the different aerosol constituents are shown in Figure S5. During P1, diurnal variations were clearly observed, with high concentrations during the nighttime and low concentrations during

the daytime because of the increased boundary layer height, enhanced mixing, and evaporation of volatile species like ammonium nitrate due to higher temperature. A relatively smaller decrease in the concentrations of sulfate and organics was observed, most likely because of the photochemical production of these species. Diurnal variations for different aerosol species were not as evident for P2 as they were for P1, most likely because of lower photochemical activities and smaller changes between the boundary layer heights during the daytime and nighttime for P2 relative to P1. The sulfate concentration peaked at approximately 10 A.M. local time during P2, as photochemical activity resumed after the fog dissipated. On average, the NO_3/SO_4 ratios were lower during P2 as compared to P1, which may be attributed to enhanced sulfate formation via fog processing. As discussed below, a sharp increase in the OA during P2 nighttime was resulted from the combined effect of the enhanced biomass burning activities and lower boundary layer heights.

The aerosol neutralization ratio (ANR) was defined in terms of the AMS measured (m) NH_4^+ to predicted (p) NH_4^+ ratio [*Zhang et al*., 2007a] as follows:

$$\mathrm{ANR} = \mathrm{NH_4^+measured}(m)/\mathrm{NH_4^+predicted}(p)\mathrm{ratio} = \frac{\mathrm{NH_4^+}(m)/18}{\frac{\mathrm{NO_3^-}(m)}{62} + 2^{*}\frac{\mathrm{SO_4^{-2}}(m)}{98} + \frac{\mathrm{Cl^-}(m)}{35.5}}$$

where NH_4^+ (m), SO_4^{-2} (m), NO_3^- (m), and Cl^- (m) are the measured AMS mass concentrations of ammonium, sulfate, nitrate, and chloride, respectively, and NH_4^+ (p) is the predicted mass concentration of ammonium that was obtained by assuming that ammonium was the only cation that balanced the anions. Other cations, such as Ca^{+2} and Mg^{+2}, can also contribute to aerosol neutralization; however, previous studies conducted at the same location [*Ram and Sarin*, 2011] have shown that most of these metallic cations are associated with coarse mode (>2.5 μm) particles; thus, the assumption that NH_4^+ is the dominant cation in the submicron aerosol is reasonable.

Generally, aerosols from both the periods were neutralized (average P1 ANR = 1.01 ± 0.09, average P2 ANR = 0.96 ± 0.10) (see Figure S6 in the supporting information). The enhanced conversion of NH_3 to NH_4^+ at low temperatures and high RH [*Seinfeld and Pandis*, 2006], and abundance of NH_3 in this region [*Behera and Sharma*, 2010a; *Ram et al*., 2012; *Behera et al*., 2013] may have led to the neutralization of aerosols at this location.

Organonitrates (ON) can also produce NO^+ and NO_2^+ fragments and affect acidity calculations [*Farmer et al*., 2010]. However, in this study, the average NO^+/NO_2^+ ratio varied between 2 and 2.7. This value was very similar to the ratio (2–2.30) obtained for pure NH_4NO_3 during the IE calibrations and much lower than the values reported for ON in other AMS studies [*Fry et al*., 2009; *Bruns et al*., 2010]. High RH values (>50%) during both seasons were unfavorable for ON formation because of enhanced hydrolysis [*Liu et al*., 2012]. Thus, contribution of ONs seemed to be small or absent.

3.2. OA Source Apportionment Via PMF

A PMF was performed on the AMS OA mass spectra for the entire study period using the HR V mode data. P2 and P1 periods were combined to identify the common factors that were present during both the periods and the variations in the contributions of these factors between the periods. The combined HR-PMF was used to divide the total OA into six factors (Figure 2), two primary BBOA (biomass burning OA), one HOA (hydrocarbon-like OA), and three OOA factors (oxidized OA, a surrogate of SOA), including one aged/oxidized BBOA [*Ng et al*., 2011] factor. PMF diagnostics are presented in the supporting information Figure S7. Except BBOA, the other factors were chosen based on the Q/Q_{exp} values, the residuals, the physical interpretability, and the correlations with external tracers (Figure S8). No external tracers are available for BBOA; however, time trends of all the BBOA components exhibited good correlations with m/z 60 (the fragment that is used as a biomass burning marker in the AMS spectra) during both the periods. Relatively less oxidized biomass burning factors, BBOA-1 and BBOA-2, likely reflected the primary BBOA emissions, whereas the more oxidized OOA_3-BBOA is hypothesized to reflect the BBOA emissions that were aged and underwent ambient processing. The diurnal plots (Figures 3a and 3b) of the PMF factors during P2 exhibited a sharp increase in the BBOA-1 and BBOA-2 concentrations during the night due to enhanced local biomass burning activities. Although time series of BBOA-1 and BBOA-2 looks similar, Figure S3 shows that BBOA-1 has a larger contribution from m/z 44 than BBOA-2, possibly due to the presence of higher levels of carboxylic

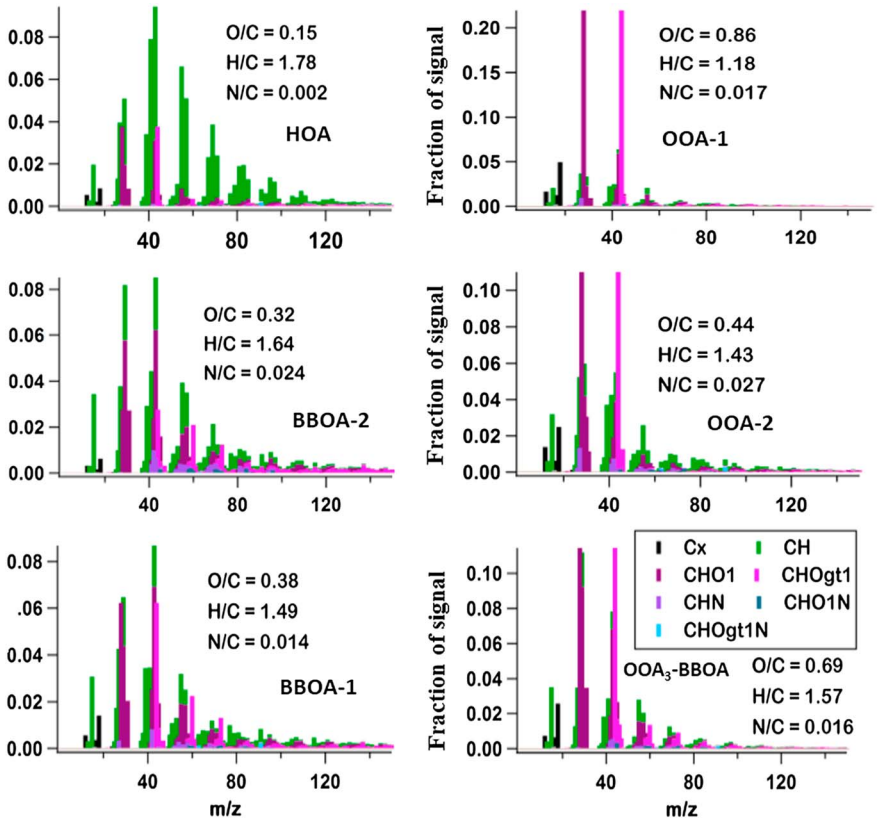

Figure 2. Combined HR-PMF factor profiles. OOA-1 and OOA-2 = oxidized organic aerosol factors, HOA = hydrocarbon-like OA (primary OA), BOOA-1 and BOOA-2 = biomass burning OA, and OOA_3-BBOA = oxidized/aged BBOA.

acid moieties [*Ng et al.*, 2011] in its molecular composition. The difference in the chemical composition of the two primary BBOAs likely reflects either two different types of biomass sources and/or different burning conditions of the same type of biomass. Highly oxidized BBOA factors have been reported in other studies [*Healy et al.*, 2013; *Timonen et al.*, 2013]. On average, increase in the absolute OA loading from P1 to P2 primarily occurred because of the higher contributions of the BBOA-2 and OOA_3-BBOA components (Figure 3b). The diurnal time trends and the correlations between HOA and black carbon (see Figure S8) suggest that HOA was mainly coming from vehicular emissions. The HOA O/C ratio (0.15) calculated from the apportioned time trends was greater than that reported for diesel/gasoline exhaust [*Mohr et al.*, 2009]. However, similar values have been reported in previous measurements [*Aiken et al.*, 2010; *Huang et al.*, 2010] of HOA in Mexico and China. It is important to note, however, that the HOA mass spectrum observed in this study may have contributions from unresolved cooking organic aerosol (COA). This is suggested by a higher m/z 55/57 ratio (=1.4) than usually seen for HOA (~1) [*Mohr et al.*, 2009; *Allan et al.*, 2010] and a significant contribution from the oxidized fragment ($C_3H_3O^+$) to m/z 55 which are more typically associated with the COA [*Allan et al.*, 2010; *Zhang et al.*, 2015]. HOA and COA may not be separated by PMF analysis (even when using solutions with higher numbers of factors) possibly due to their emission from sources with similar temporal trends. Other ambient studies [*He et al.*, 2010, 2011] also reported this difficulty in separating OA factors with similar temporal trends and could explain the slightly higher O/C ratio of the HOA. The separation of HOA by PMF in air masses that are impacted by BBOA (particularly in the winter) is difficult and contributed some uncertainty to the source apportionment of the HOA factor mass spectrum and the time series.

The OOA-1 time trend was better correlated with odd oxygen O_X ($O_3 + NO_2$) [*Wood et al.*, 2010] during P2 as compared to P1, suggesting that OOA-1 was produced by local photochemistry. Although the peak in OOA-1 was not as obvious in the afternoons of P1, the OOA-1 concentrations remained constant despite the distinct increase in the boundary layer height in the afternoon, consistent with local photochemical production of OOA-1 during this period.

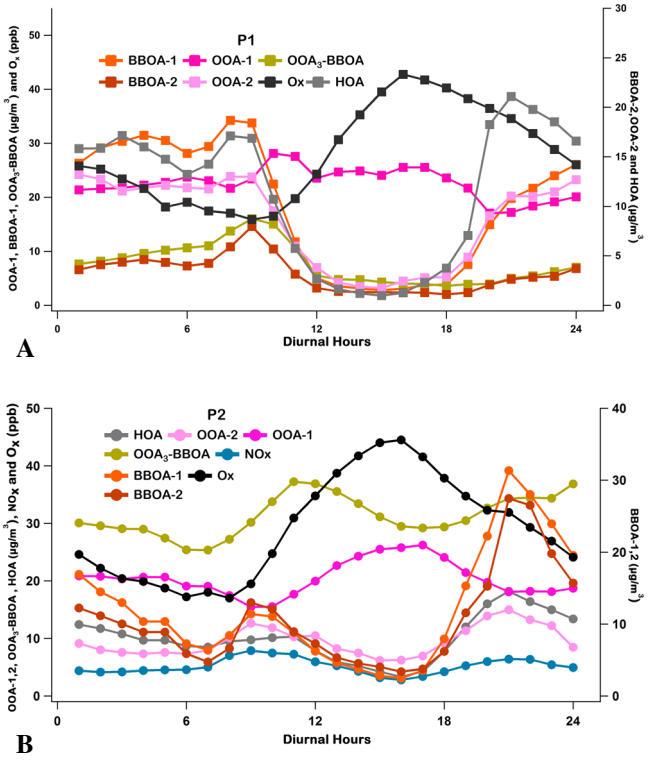

Figure 3. (a) HR-PMF factor diurnal profiles during P1. (b) HR-PMF factor diurnal profiles during P2; hourly NOX data were only available during P2. Decreasing trend during afternoon indicates increased boundary layer height (BLH) while nighttime increase indicates a combination of low BLH with enhanced local emissions.

The OOA-2 time series was well correlated with that of the aerosol nitrate indicating semivolatile nature of this oxidized factor. During P2 period, the secondary OAs (OOA1,2 + OOA_3-BBOA, 69%) contributed significantly more toward the total OA than the primary OAs (29%, HOA + BBOA1,2) (Figures 1b and S9). However, the secondary and primary OA contributed equally during P1 (2% of the mass remained unapportioned in the PMF). Basic PMF diagnostics and correlations with external tracers are shown in the supporting information (Figures S7 and S8). The PMF analysis also shows that the OA composition varied significantly, although the overall NR-PM_1 composition did not change significantly from P1 to P2 (Figure 1b).

3.3. Back Trajectory Analysis

The effects of regional and long-range transport on NR-PM_1 aerosol loading and composition were determined by performing a back trajectory (BT) analysis using the Hybrid Single-Particle Lagrangian Integrated Trajectory (HYSPLIT4) model developed by NOAA/Air Resources Laboratory (ARL) [*Draxler and Rolph*, 2003]. The meteorological data used in the computation of the trajectories come from the Global Data Assimilation System archive maintained by ARL (available online at http://ready.arl.noaa.gov/archives.php). First, 48 h back trajectories starting at 500 m above the ground in Kanpur (26.46°N, 80.33°E) were calculated every hour throughout the study period. Next, the trajectories were clustered according to their similarities in terms of spatial distributions using HYSPLIT4 software. The clustering principles and processes are described in the software user guide [*Draxler et al.*, 2014]. The five-cluster (denoted as C1 to C5) solution was considered optimum for clustering according to the change in the total spatial variance, and the mean BTs of each cluster are shown in Figure 4. After clustering, the PM_1 chemical compositions corresponding to the BTs in each cluster were averaged, which is also shown in Figure 4. The BT analysis confirmed that the air masses sampled in this study predominantly arrived from the northwest, as reported in a previously conducted wintertime study at this location [*Patidar et al.*, 2012]. BT analysis also indicates that the site is primarily affected by surface emissions as evident from the trajectory heights (Figure S10). However, the BT analysis also revealed some differences between P2 and P1. During P2, apart from C4 and C5, all other air masses had arrived from much longer distances away (>1000 km) relative to those that arrived during P1, and the most polluted air was associated with cluster 3, which had the highest contributions of biomass burning aerosols and sulfate. As previously mentioned, paddy residue is burned every year throughout northwest India in November, and these burning events affect the air masses transported to Kanpur. The NASA Moderate Resolution Imaging Spectroradiometer (MODIS) fire map [*Giglio et al.*, 2003] indicated the presence of burning near the origin of the C3 air mass, which caused high loadings. Short-range regional transport also appeared to contribute to the NR-PM_1 loading, as indicated by C2. The lowest aerosol concentrations were observed for the C1 air masses, which underwent short-range transport but originated from southeast of the site. During P2, C1 represented the aerosols transported across the longest ranges and originated in northwest Pakistan. This cluster contained the highest relative contributions from OOA-1 but had the lowest aerosol concentration of all the clusters. In addition, C1 contained the highest relative amount of nitrate and the lowest relative contributions from sulfate among the five clusters. The air mass

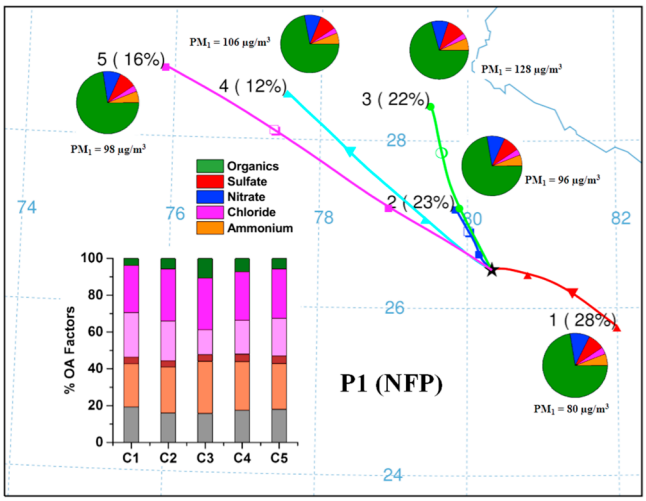

A

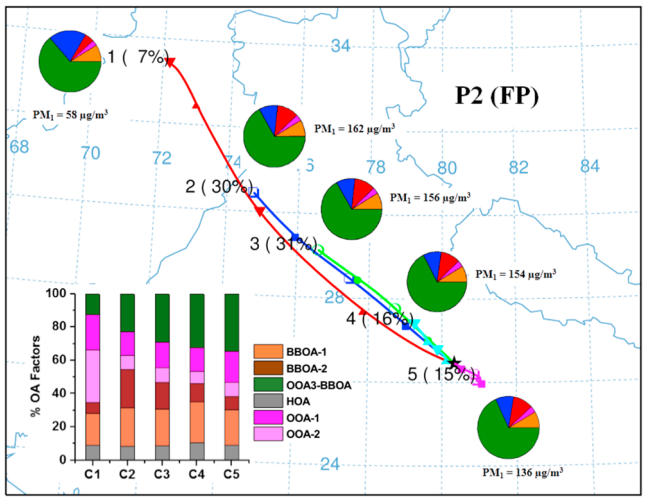

B

Figure 4. (a) Back trajectory analysis for P1. During P1 air masses were arriving from much shorter distances than P2. Pie and bar charts are showing average NR-PM1 composition and relative contributions of different types of OA, respectively. (b) Back trajectory analysis for P2. During P2 air masses were arriving from much longer distances P1 (Figure 4a). Pie and bar charts are showing average NR-PM1 composition and relative contributions of different types of OA, respectively.

traveled over several coal mines located in the area in Pakistan. Normally, coal mines are associated with huge NO_x emissions from heavy mining equipment and nonideal burning of ammonium nitrate used in blasting [*Attalla et al.*, 2008], which could result in relatively high nitrate contributions.

Apart from C1, all of the clusters during P2 had smaller contributions from OOA-1 and OOA-2, likely due to the stagnant conditions and lower levels of photochemical activity. Other clusters during P2 were significantly affected by the biomass burning-related sources. For example, C2 contained the highest relative contributions from the primary BBOA fractions and the most polluted air mass. These observations were consistent with the NASA MODIS fire map [*Giglio et al.*, 2003] of fire events in the path of this air mass. Short-range regional transport (as represented by C4 and C5) appeared to contribute substantially to P2, and these air masses received their highest contributions from the aged BBOA fraction. The relative contributions of the aged BBOA increased as the air mass transport range decreased, and the highest oxidized BBOA contributions were observed during actual fog events. These observations suggest the need for future investigations to determine whether fog plays a role in primary BBOA processing at the study location.

3.4. Organic Aerosol Elemental Ratios and Processing

3.4.1. Difference Between P2 and P1

The organic aerosol elemental ratios exhibited stronger diurnal patterns (Figure 5) during P1 than P2, and the O/C ratio peaked in the afternoon, indicating strong photochemical activity. But during P2, the daytime O/C ratio was only slightly higher than the nighttime O/C ratio (Figure 5). Generally, the primary organic aerosol species (HOA and BBOA) with higher H/C and lower O/C values, were more dominant at nighttime compared to daytime. The N/C ratio was slightly higher during P2, mostly resulted from the enhanced contributions from biomass burning [*Laskin et al.*, 2009; *Huang et al.*, 2011] and/or the interactions of the organics with NH_3.

While solar radiation was higher during P1 (the average solar radiation was 463 ± 48 W/m^2 for P1 and 405 ± 51 W/m^2 for P2), the OA loading was lower during P1 (the overall and nighttime average OA values were 72 ± 30 µg/m^3 and 80 ± 34 µg/m^3, respectively, for P1 and 94 ± 32 µg/m^3 for P2_FP; the differences are statistically significant at the 95% confidence level, $p < 0.01$). Although the higher solar radiation favors more intense photochemistry and lower OA loadings favor the partitioning of relatively more oxidized organics into particulate phase than higher OA loadings [*Shilling et al.*, 2009; *Kang et al.*, 2011], the overall

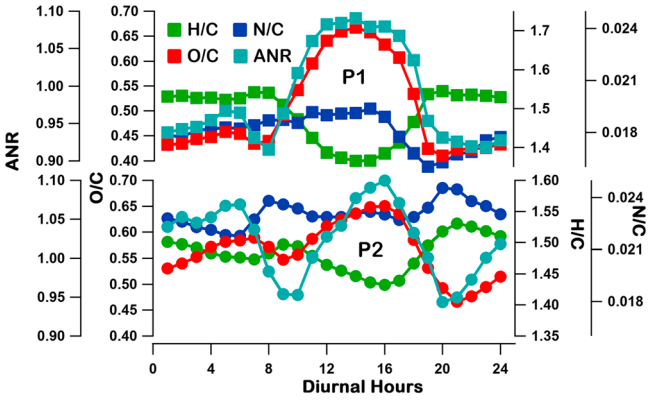

Figure 5. Diurnal variation of different elemental ratios during P2 and P1. Significant differences between daytime and nighttime O/C ratio can be seen in P1, but the differences were less during P2.

aerosol oxidation level of P1 (average O/C = 0.50) remained slightly lower than P2 (average O/C = 0.55). During P2_FP, the average nighttime (6 P.M. to 6 A.M.) O/C ratio of [0.54(±0.05)] was higher than that of nighttime P1 [0.44(±0.06)] (The differences in O/C ratios are statistically significant, $p < 0.001$) (Figure 5).

The OA evolution processes, in addition to the O/C ratio, were examined. Van Krevelen (VK) diagrams (Figure 6) have been previously used to investigate the OA chemical evolution [*Heald et al.*, 2010; *Ng et al.*, 2011]. The VK diagram shows further differences in the elemental compositions between P2 and P1. First, for any given O/C values, P2 aerosols had higher H/C values than P1 aerosols, which can be explained by enhanced contribution of OOA_3-BBOA to total OA during P2 than P1. The OOA_3-BBOA not only had a high O/C ratio but also a high H/C ratio, unlike OOA-1 (see Figure 2), which was the dominant oxidized species during P1. These factors were plotted on an f44 versus f43 "triangle" plot (Figure S3) [*Ng et al.*, 2010], which clearly showed that OOA-1 was the most aged factor at the top of the triangle and although OOA_3-BBOA had a higher O/C ratio than OOA-2, OOA_3-BBOA had a similar f44 level and a larger f43 level than OOA-2. This result suggests that oxygenated functional groups other than carboxylic groups, such as ketone/aldehyde groups [*Hawkins and Russell*, 2010] or alcohol groups, as evidenced by the higher f29 level [*Canagaratna et al.*, 2014] contributed to the high O/C values of OOA_3-BBOA. Figure 6 also shows the differences in the VK slopes for daytime and nighttime periods during P2 and P1. The OA observed during P2 lie along a shallower VK slope (−0.5) than the OA observed during P1 (−0.7). A shallower slope is consistent with P2 OA containing more −OH/−ROOH functionality than P1 OA [*Ng et al.*, 2011].

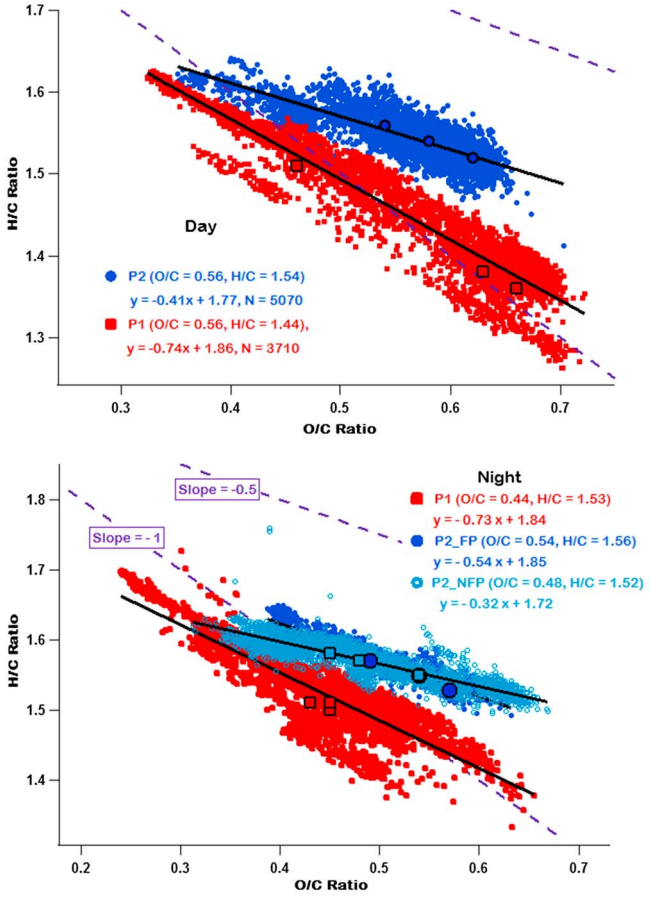

Figure 6. Slopes of Van Krevelen (VK) diagram is very different from P1 to P2 indicating differences between P2 and P1 OA evolution processes. Black bordered circles and squares are representing every consecutive 4 h average of O/C and H/C for day (6 A.M. to 10 A.M. to 2 P.M. to 6 P.M.) and night (6 P.M. to 10 P.M. to 2 A.M. to 6 A.M.), and their movement is from left to right.

A similar trend was reported in an AMS study conducted in Hong Kong during fog and haze episodes [*Li et al.*, 2013]. Figure 6 also revealed continuous chemical evolution of OA toward higher oxygenation with time during P2, while no such indication was found during P1 nights. Stagnant conditions during P2 nights along with high RH and fog seemed to have allowed more time for chemical processing of OA.

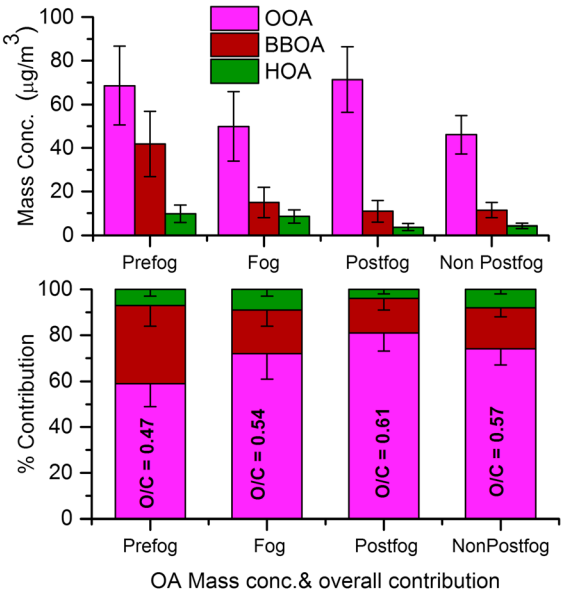

Figure 7. OA mass concentration(s) and relative composition comparison between before (6 h before fog starts), during and after fog (daytime hours after fog dissipation), and nonpostfog indicates daytime hours not preceded by a fog event. O/C and relative oxidized OA contribution to total OA increases during fog despite of fog scavenging and removal. Error bars are for ± 1 standard deviation (std) (for lower panel only −1 std is shown).

We have also looked into the daytime and nighttime variations in VK diagram slopes. While the average daytime O/C (=0.56) for P1 and P2 are similar to each other, the average nighttime O/C for P1 (=0.44) is lower than the corresponding value for P2 (=0.54) (see Figure 5). During P2 and P1, the nighttime contribution of POAs was relatively higher than daytime as many POAs (like BBOA) emissions are enhanced during night. Even with different POA:OOA ratios, the daytime and nighttime VK slopes for P1 (−0.74 and −0.73, respectively) are similar to each other, but as can be seen from Figure 6, during P1 nights, no temporal variations in H/C and O/C ratios are present indicating that different H/C, O/C values of this scatterplot are most likely originating from physical mixing of different OA components rather than any continuous OA evolution from lower to higher O/C ratio as seen for P1 daytime. For P2, daytime and nighttime slopes (−0.41 and −0.54, respectively) are slightly different but both are much shallower than that of P1; this could be due to different mixing ratios of OA components between two periods and/or difference in OA evolution processes. Shallower slope generally indicates addition of more –OH/−COOH functionality to carbon backbone while steeper slope indicates addition of more carbonyl (aldehyde/ketone) moieties [*Heald et al*., 2010; *Ng et al*., 2011]. Apart from that for P2 nights, continuous OA evolution from lower to higher O/C ratio can be seen indicating a continuous process of OA oxidation. During P2, nights were more stagnant as compared to P1 with very low wind speed and low boundary layer heights which possibly allowed more time for gas- and aqueous-phase oxidation. Although the AMS mostly measures the unscavenged and unactivated interstitial aerosols during the fog events, but it can also sample residual aerosols that have undergone aqueous processing and are left behind when fog evaporates. In this study, the large contribution from the aged BBOA factor during P2 makes it difficult to attribute enhanced oxidation to aqueous fog chemistry alone; the moderate RH and O/C correlation during P2 (Figure S11) could, however, indicate that aqueous oxidation played a part in the observed aerosol oxidation.

3.4.2. Variation in OA Composition and Elemental Ratios Within P2 (FP)

During P2 periods both foggy and nonfoggy time periods were observed. In general, the OA composition was different between these two types of P2 periods (Figure S12) with P2_FP (O/C = 0.54) being more enriched in OOA than P2_NFP nights (O/C = 0.48). The OA from P2_FP and P2_NFP nights also lie along different slopes in the VK diagram (−0.54 versus −0.32, respectively) (Figure 6). To assess whether this difference was due to differences in nature of OA chemical evolution or only caused by physical mixing of different OA components, we have replotted the VK diagrams for P2_FP and P2_NFP nights categorized according to similar ranges of POA:OOA ratios: 0–30%, 30–60%, and 60–100% (Figure S13). We found that VK diagram slopes for P2_FP (−0.40, −0.32, −0.37) and P2_NFP nights(−0.50, −0.70) (Figure S13) differ even for conditions with similar POA:OOA ratios and for P2_NFP nights physical mixing have little effect on VK slopes. This suggests that the differences in OA chemical composition during P2_FP and P2_NFP could also be due to differences in chemical processing due to the presence/absence of fog.

A detailed analysis of prefog, fog, and postfog time periods (Figure 7) is used to elucidate the effect of fog on the OA composition. Prefog period is taken as 6 h before the onset of fog and postfog period as the daytime hours after fog dissipation. There were a few instances when fog events occurred on back-to-back days, so to avoid overlapping between prefog and postfog hours, this scheme is chosen. So prefog + foggy time periods were essentially evening to early morning periods, whereas postfoggy periods were mostly daytime hours.

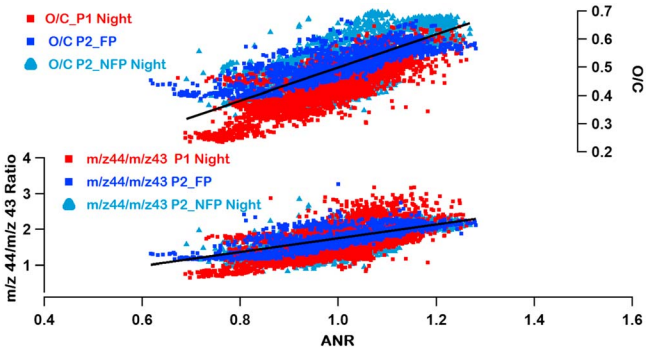

Figure 8. Relationships between the O/C and m/z44/m/z43 ratios and the ANR, which were well correlated with aerosol neutralization during both the periods (including the daytime, not shown).

Daytime hours during P2 that were not preceded by any fog events are classified as nonpostfoggy time periods.

As shown in Figure 7 apart from a very marginal decrease in HOA, all other OA components decreased significantly during fog periods as compared to prefog periods due to fog scavenging and removal. But the relative decrease (~70%) in primary BBOAs was much higher than OOAs (OOA1,2 + OOA_3-BBOA) (~30%). So the relative contributions of OOAs increased from prefog to foggy period (increase is statistically significant, $p < 0.01$) in line with the observed O/C increase. While more oxidized and hygroscopic OOA is expected to be preferentially scavenged as compared to primary BBOA [*Gilardoni et al*., 2014] it is likely that the OOA scavenging is offset by the OOA production.

Generally, stagnant and calm conditions during fog reduces the importance of long-range transport [*Jacob et al*., 1967; *Dall'Osto et al*., 2008], so the additional observed OOA was likely produced locally via enhanced aqueous (fog) phase processing [*Kaul et al*., 2011] along with usual gas-phase oxidation at this location. After fog dissipation and in the presence of the Sun, OOA increased while HOA and BBOA decreased possibly due to increased boundary layer height. It is also interesting to note that the OOA mass concentration during nonpostfoggy days were much lower than during postfoggy days while POAs mass concentration remained the same (Figure 7); as a consequence, nonpostfoggy OA had a lower O/C ratio and lower relative contribution (both are statistically significantly lower) from OOAs than postfoggy days. Unchanged POA concentration from postfoggy to nonpostfoggy days indicates that boundary layer dynamics did not play an important role in the observed change in OOA concentration. Instead, it is possible that the higher OOA concentration during postfoggy days was caused by enhanced amounts of oxidized organic residues left behind after fog evaporation.

3.4.3. ANR Versus O/C Relationship

Figure 8 clearly shows that the ANR was correlated with the O/C, where the O/C increased with the ANR over both the periods. The diurnal variations of the O/C appeared to be closely correlated with the aerosol acidity (Figure 5). In a recent laboratory study using an AMS [*Liggio and Li*, 2013], the O/C ratio was reported to increase immediately after aerosol neutralization with excess NH_3, which was attributed to the formation of oxidized oligomers ($m/z > 300$) in the aerosol phase. Such a link was not clearly observed since possible oligomers were fragmented in the AMS. During P2 and P1, the increase in the O/C in the afternoon was associated with increasing relative intensity of the high m/z 44 (CO_2^+) signal that is known to originate from carboxylic acids in the AMS [*Alfarra*, 2004; *Takegawa et al*., 2007]. Thus, the positive correlation between the O/C ratio and the ANR during the daytime may indicate the association of excess NH_4^+ with organic acids.

4. Conclusions

We report the first use of an HR-ToF-AMS in India for obtaining real-time measurements of submicron aerosol characteristics. This study was conducted in a highly polluted Indian city during the winter. The results revealed extremely high NR-PM_1 loadings that were much greater than previously reported in other AMS studies. The overall aerosol composition was overwhelmingly dominated by organics throughout this study. Although the overall aerosol composition between P2 and P1 was similar, the source apportionment of OA via PMF revealed significant differences in the OA composition between the two periods. Particularly, the aged biomass burning factor contributed a significant portion of the OA during the foggy period. Local photochemical formation of oxidized organic aerosols was observed during the afternoon for both the periods. Van Krevelen plots of the aerosol composition showed continuous increase in O/C ratio throughout the P2 nights but revealed no such change during P1 nights. Also, the changes in OA elemental ratios/OA evolution followed different slopes during P1 and P2, even within P2 slopes are different from foggy to

nonfoggy nights. This change in slope cannot be explained by physical mixing of different OA factors alone and indicates that the changes in nature of oxidized functional groups added to OA during oxidation. Shallower slopes during P2 indicates that more acidic (−COOH) functional groups were added to OA as compared to more carbonyl (aldehyde and ketone) functional groups during P1 with much steeper slopes. A strong correlation between the aerosol oxidation level and aerosol neutralization was observed during this study. Increases in the ANR were largely correlated with increase in O/C and m/z 44 intensity (an AMS signature of the aerosol organic acid content) in the spectra, suggesting some interactions between the organic acids and inorganics. The time-resolved measurements in this study provide us with new information that has not been reported previously from traditional offline filter measurements conducted at the same location. We still lacked some valuable information on gas-phase chemistry, so future work will include the deployment of other real-time instruments like PTR-MS for measurements of VOC's with gas-phase OA oxidation and analysis of collected fog water. These additional measurements will offer a complete picture of effects of fog processing on gas + aqueous + condensed-phase OA in this highly populated and polluted region.

Acknowledgments

We acknowledge the support of IIT Kanpur for providing us with an HR-ToF-AMS for PG research and teaching. We also acknowledge funding by the Department of Science and Technology (DST) in India under the Continental Tropical Convergence Zone climate change program of the DST. We are grateful to Puneet Chhabra and Donna Super for their assistance with the HR and PMF data analysis. In addition, we thank Leah Williams and Vijay P. Kanwade for their input and acknowledge the NASA-AERONET-Solar Radiation Network team for providing us with solar flux data for Kanpur. We acknowledge the NOAA Air Resources Laboratory (ARL) for providing us with the HYSPLIT transport and dispersion model. The data that were used in Figure 4 were obtained from the NOAA website (http://ready.arl.noaa.gov). All the data and results that are used to support the conclusions of this article can be obtained from corresponding authors by sending emails to tarun@iitk.ac.in and/or snt@iitk.ac.in. This article contains supporting information that is 11 pages long (Text S1) with 13 figures (Figures S1–S13) and one table.

References

Aiken, A. C., P. F. DeCarlo, and J. L. Jimenez (2007), Elemental analysis of organic species with electron ionization high-resolution mass spectrometry, *Anal. Chem.*, *79*(21), 8350–8358, doi:10.1021/ac071150w.

Aiken, A. C., et al. (2008), O/C and OM/OC ratios of primary, secondary, and ambient organic aerosols with high-resolution time-of-flight aerosol mass spectrometry, *Environ. Sci. Technol.*, *42*(12), 4478–4485, doi:10.1021/es703009q.

Aiken, A. C., et al. (2010), Mexico City aerosol analysis during MILAGRO using high resolution aerosol mass spectrometry at the urban supersite (T0)—Part 2: Analysis of the biomass burning contribution and the non-fossil carbon fraction, *Atmos. Chem. Phys.*, *10*(12), 5315–5341, doi:10.5194/acp-10-5315-2010.

Alfarra, M. (2004), Insights into atmospheric organic aerosols using an aerosol mass spectrometer, PhD thesis, Inst. of Sci. and Technol., Univ. of Manchester, Manchester, U. K.

Alfarra, M. R., et al. (2004), Characterization of urban and rural organic particulate in the lower Fraser valley using two aerodyne aerosol mass spectrometers, *Atmos. Environ.*, *38*(34), 5745–5758, doi:10.1016/j.atmosenv.2004.01.054.

Allan, J. D. (2003), Correction to "Quantitative sampling using an aerodyne aerosol mass spectrometer: 1. Techniques of data interpretation and error analysis", *J. Geophys. Res.*, *108*(D9), 4283, doi:10.1029/2003JD001607.

Allan, J. D., P. I. Williams, W. T. Morgan, C. L. Martin, M. J. Flynn, J. Lee, E. Nemitz, G. J. Phillips, M. W. Gallagher, and H. Coe (2010), Contributions from transport, solid fuel burning and cooking to primary organic aerosols in two UK cities, *Atmos. Chem. Phys.*, *10*(2), 647–668.

Attalla, M. I., S. J. Day, T. Lange, W. Lilley, and S. Morgan (2008), NO_x emissions from blasting operations in open-cut coal mining, *Atmos. Environ.*, *42*(34), 7874–7883.

Bahreini, R., et al. (2009), Organic aerosol formation in urban and industrial plumes near Houston and Dallas, Texas, *J. Geophys. Res.*, *114*, D00F16, doi:10.1029/2008JD011493.

Behera, S. N., and M. Sharma (2010a), Investigating the potential role of ammonia in ion chemistry of fine particulate matter formation for an urban environment, *Sci. Total Environ.*, *408*, 3569–3575, doi:10.1016/j.scitotenv.2010.04.017.

Behera, S. N., and M. Sharma (2010b), Reconstructing primary and secondary components of PM2.5 composition for an urban atmosphere, *Aerosol Sci. Technol.*, *44*(11), 983–992, doi:10.1080/02786826.2010.504245.

Behera, S. N., M. Sharma, V. P. Aneja, and R. Balasubramanian (2013), Ammonia in the atmosphere: A review on emission sources, atmospheric chemistry and deposition on terrestrial bodies, *Environ. Sci. Pollut. Res.*, *20*, 8092–8131, doi:10.1007/s11356-013-2051-9.

Bhattu, D., and S. N. Tripathi (2015), CCN closure study: Effects of aerosol chemical composition and mixing state, *J. Geophys. Res. Atmos.*, *120*, 766–783, doi:10.1002/2014JD021978.

Bond, T. C., D. G. Streets, K. F. Yarber, S. M. Nelson, J. H. Woo, and Z. Klimont (2004), A technology-based global inventory of black and organic carbon emissions from combustion, *J. Geophys. Res.*, *109*, D14203, doi:10.1029/2003JD003697.

Bruns, E. A., V. Perraud, A. Zelenyuk, M. J. Ezell, S. N. Johnson, Y. Yu, D. Imre, B. J. Finlayson-Pitts, and M. L. Alexander (2010), Comparison of FTIR and particle mass spectrometry for the measurement of particulate organic nitrates, *Environ. Sci. Technol.*, *44*(3), 1056–1061, doi:10.1021/es9029864.

Canagaratna, M. R., et al. (2004), Chase studies of particulate emissions from in-use New York City vehicles, *Aerosol Sci. Technol.*, *38*(6), 555–573, doi:10.1080/02786820490465504.

Canagaratna, M. R., et al. (2007), Chemical and microphysical characterization of ambient aerosols with the aerodyne aerosol mass spectrometer, *Mass Spectrom. Rev.*, *26*(2), 185–222, doi:10.1002/mas.20115.

Canagaratna, M. R., et al. (2014), Elemental ratio measurements of organic compounds using aerosol mass spectrometry: Characterization, improved calibration, and implications, *Atmos. Chem. Phys. Discuss.*, *14*(13), 19,791–19,835, doi:10.5194/acpd-14-19791-2014.

Cheng, Z., et al. (2014), Impact of biomass burning on haze pollution in the Yangtze River delta, China: A case study in summer 2011, *Atmos. Chem. Phys.*, *14*(9), 4573–4585, doi:10.5194/acp-14-4573-2014.

Dall'Osto, M., R. M. Harrison, H. Coe, and P. Williams (2008), Real-time observation of secondary aerosol formation during a fog event in London, *Atmos. Chem. Phys. Discuss.*, *8*, 20,019–20,050, doi:10.5194/acpd-8-20019-2008.

De Gouw, J., and J. L. Jimenez (2009), Organic aerosols in the Earth's atmosphere, *Environ. Sci. Technol.*, *43*(20), 7614–7618, doi:10.1021/es9006004.

DeCarlo, P. F., et al. (2006), Field-deployable, high-resolution, time-of-flight aerosol mass spectrometer, *Anal. Chem.*, *78*(24), 8281–8289, doi:10.1021/ac061249n.

Deng, X., X. Tie, D. Wu, X. Zhou, X. Bi, H. Tan, F. Li, and C. Jiang (2008), Long-term trend of visibility and its characterizations in the Pearl River Delta (PRD) region, China, *Atmos. Environ.*, *42*, 1424–1435, doi:10.1016/j.atmosenv.2007.11.025.

Draxler, R., and G. D. Rolph (2003), HYSPLIT (HYbrid Single-Particle Lagrangian Integrated Trajectory) model, access via NOAA ARL READY Website (http://www.arl.noaa.gov/ready/hysplit4.html), NOAA Air Resources Lab., Silver Spring, Md.

Draxler, R., B. Stunder, G. Rolph, A. Stein, and A. Taylor (2014), HYSPLIT4 user's guide, Version 4. Last Revised September 2014. [Available at http://www.arl.noaa.gov/documents/reports/hysplit_user_guide.pdf.]
Drewnick, F., et al. (2005), A new time-of-flight aerosol mass spectrometer (TOF-AMS)—Instrument description and first field deployment, *Aerosol Sci. Technol.*, *39*, 637–658, doi:10.1080/02786820500182040.
Farmer, D. K., A. Matsunaga, K. S. Docherty, J. D. Surratt, J. H. Seinfeld, P. J. Ziemann, and J. L. Jimenez (2010), Response of an aerosol mass spectrometer to organonitrates and organosulfates and implications for atmospheric chemistry, *Proc. Natl. Acad. Sci. U.S.A.*, *107*(15), 6670–6675, doi:10.1073/pnas.0912340107.
Frank, G., et al. (1998), Droplet formation and growth in polluted fogs, *Contrib. Atmos. Phys.*, *71*(1), 65–85.
Fry, J. L., et al. (2009), Organic nitrate and secondary organic aerosol yield from NO_3 oxidation of β-pinene evaluated using a gas-phase kinetics/aerosol partitioning model, *Atmos. Chem. Phys.*, *9*(4), 1431–1449, doi:10.5194/acp-9-1431-2009.
Giglio, L., J. Descloitres, C. O. Justice, and Y. J. Kaufman (2003), An enhanced contextual fire detection algorithm for MODIS, *Remote Sens. Environ.*, *87*, 273–282, doi:10.1016/S0034-4257(03)00184-6.
Gilardoni, S., et al. (2014), Fog scavenging of organic and inorganic aerosol in the Po Valley, *Atmos. Chem. Phys.*, *14*(13), 6967–6981, doi:10.5194/acp-14-6967-2014.
Government of India (2011), Indian census 2011. [Available at http://www.census2011.co.in/census/district/535-kanpur-nagar.html.]
Grieshop, A. P., J. M. Logue, N. M. Donahue, and A. L. Robinson (2009a), Laboratory investigation of photochemical oxidation of organic aerosol from wood fires—1: Measurement and simulation of organic aerosol evolution, *Atmos. Chem. Phys.*, *9*(4), 1263–1277.
Grieshop, A. P., N. M. Donahue, and A. L. Robinson (2009b), Laboratory investigation of photochemical oxidation of organic aerosol from wood fires—2: Analysis of aerosol mass spectrometer data, *Atmos. Chem. Phys.*, *9*(6), 2227–2240.
Gupta, A. K., S. Nag, and U. K. Mukhopadhyay (2006), Characterisation of PM10, PM2.5 and benzene soluble organic fraction of particulate matter in an urban area of Kolkata, India, *Environ. Monit. Assess.*, *115*(1–3), 205–222, doi:10.1007/s10661-006-6550-8.
Gupta, T., and A. Mandariya (2013), Sources of submicron aerosol during fog-dominated wintertime at Kanpur, *Environ. Sci. Pollut. Res.*, *20*(8), 5615–5629, doi:10.1007/s11356-013-1580-6.
Gurjar, B. R., J. A. van Aardenne, J. Lelieveld, and M. Mohan (2004), Emission estimates and trends (1990–2000) for megacity Delhi and implications, *Atmos. Environ.*, *38*(33), 5663–5681, doi:10.1016/j.atmosenv.2004.05.057.
Hallquist, M., et al. (2009), The formation, properties and impact of secondary organic aerosol: Current and emerging issues, *Atmos. Chem. Phys.*, *9*(14), 5155–5236.
Hawkins, L. N., and L. M. Russell (2010), Oxidation of ketone groups in transported biomass burning aerosol from the 2008 Northern California Lightning Series fires, *Atmos. Environ.*, *44*, 4142–4154, doi:10.1016/j.atmosenv.2010.07.036.
He, L. Y., Y. Lin, X. F. Huang, S. Guo, L. Xue, Q. Su, M. Hu, S. J. Luan, and Y. H. Zhang (2010), Characterization of high-resolution aerosol mass spectra of primary organic aerosol emissions from Chinese cooking and biomass burning, *Atmos. Chem. Phys.*, *10*(23), 11,535–11,543, doi:10.5194/acp-10-11535-2010.
He, L.-Y., X.-F. Huang, L. Xue, M. Hu, Y. Lin, J. Zheng, R. Zhang, and Y.-H. Zhang (2011), Submicron aerosol analysis and organic source apportionment in an urban atmosphere in Pearl River Delta of China using high-resolution aerosol mass spectrometry, *J. Geophys. Res.*, *116*, D12304, doi:10.1029/2010JD014566.
Heald, C. L., J. H. Kroll, J. L. Jimenez, K. S. Docherty, P. F. Decarlo, A. C. Aiken, Q. Chen, S. T. Martin, D. K. Farmer, and P. Artaxo (2010), A simplified description of the evolution of organic aerosol composition in the atmosphere, *Geophys. Res. Lett.*, *37*, L08803, doi:10.1029/2010GL042737.
Healy, R. M., et al. (2013), Quantitative determination of carbonaceous particle mixing state in Paris using single-particle mass spectrometer and aerosol mass spectrometer measurements, *Atmos. Chem. Phys.*, *13*(18), 9479–9496, doi:10.5194/acp-13-9479-2013.
Huang, X. F., et al. (2010), Highly time-resolved chemical characterization of atmospheric submicron particles during 2008 Beijing Olympic Games using an aerodyne high-resolution aerosol mass spectrometer, *Atmos. Chem. Phys.*, *10*(18), 8933–8945, doi:10.5194/acp-10-8933-2010.
Huang, X.-F., et al. (2011), Characterization of submicron aerosols at a rural site in Pearl River Delta of China using an aerodyne high-resolution aerosol mass spectrometer, *Atmos. Chem. Phys.*, *11*(5), 1865–1877, doi:10.5194/acp-11-1865-2011.
Jacob, D. J., F. H. Shair, J. M. Waldman, J. W. Munger, and M. R. Hoffmann (1967), Transport and oxidation of SO_2 in a stagnant foggy valley, *Atmos. Environ.*, *21*(6), 1305–1314, doi:10.1016/0004-6981(67)90077-7.
Jacobson, M. C., H. C. Hansson, K. J. Noone, and R. J. Charlson (2000), Organic atmospheric aerosols: Review and state of the science, *Rev. Geophys.*, *38*(2), 267–294, doi:10.1029/1998RG000045.
Jayne, J. T., D. C. Leard, X. F. Zhang, P. Davidovits, K. A. Smith, C. E. Kolb, and D. R. Worsnop (2000), Development of an aerosol mass spectrometer for size and composition analysis of submicron particles, *Aerosol Sci. Technol.*, *33*, 49–70, doi:10.1080/027868200410840.
Jimenez, J. L., et al. (2003), Ambient aerosol sampling using the aerodyne aerosol mass spectrometer, *J. Geophys. Res.*, *108*(D7), doi:10.1029/2001JD001213.
Jimenez, J. L., et al. (2009), Evolution of organic aerosols in the atmosphere, *Science*, *326*(5959), 1525–1529, doi:10.1126/science.1180353.
Joseph, A. E., S. Unnikrishnan, and R. Kumar (2012), Chemical characterization and mass closure of fine aerosol for different land use patterns in Mumbai City, *Aerosol Air Qual. Res.*, *12*(1), 61–72, doi:10.4209/aaqr.2011.04.0049.
Kang, E., D. W. Toohey, and W. H. Brune (2011), Dependence of SOA oxidation on organic aerosol mass concentration and OH exposure: Experimental PAM chamber studies, *Atmos. Chem. Phys.*, *11*(4), 1837–1852, doi:10.5194/acp-11-1837-2011.
Kaul, D. S., T. Gupta, S. N. Tripathi, V. Tare, and J. L. Collett Jr. (2011), Secondary organic aerosol: A comparison between foggy and nonfoggy days, *Environ. Sci. Technol.*, *45*(17), 7307–7313, doi:10.1021/es201081d.
Kaul, D. S., T. Gupta, and S. N. Tripathi (2012), Chemical and microphysical properties of the aerosol during foggy and nonfoggy episodes: A relationship between organic and inorganic content of the aerosol, *Atmos. Chem. Phys. Discuss.*, *12*(6), 14,483–14,524, doi:10.5194/acpd-12-14483-2012.
Lance, S., C. A. Brock, D. Rogers, and J. A. Gordon (2010), Water droplet calibration of the Cloud Droplet Probe (CDP) and in-flight performance in liquid, ice and mixed-phase clouds during ARCPAC, *Atmos. Meas. Tech.*, *3*(6), 1683–1706, doi:10.5194/amt-3-1683-2010.
Laskin, A., J. S. Smith, and J. Laskin (2009), Molecular characterization of nitrogen-containing organic compounds in biomass burning aerosols using high-resolution mass spectrometry, *Environ. Sci. Technol.*, *43*, 3764–3771, doi:10.1021/es803456n.
Li, Y. J., B. Y. L. Lee, J. Z. Yu, N. L. Ng, and C. K. Chan (2013), Evaluating the degree of oxygenation of organic aerosol during foggy and hazy days in Hong Kong using high-resolution time-of-flight aerosol mass spectrometry (HR-ToF-AMS), *Atmos. Chem. Phys.*, *13*(17), 8739–8753, doi:10.5194/acp-13-8739-2013.
Liggio, J., and S. M. Li (2013), A new source of oxygenated organic aerosol and oligomers, *Atmos. Chem. Phys.*, *13*(6), 2989–3002, doi:10.5194/acp-13-2989-2013.

Liu, P. S. K., R. Deng, K. A. Smith, L. R. Williams, J. T. Jayne, M. R. Canagaratna, K. Moore, T. B. Onasch, D. R. Worsnop, and T. Deshler (2007), Transmission efficiency of an aerodynamic focusing lens system: Comparison of model calculations and laboratory measurements for the aerodyne aerosol mass spectrometer, *Aerosol Sci. Technol.*, *41*(8), 721–733, doi:10.1080/02786820701422278.

Liu, S., J. E. Shilling, C. Song, N. Hiranuma, R. A. Zaveri, and L. M. Russell (2012), Hydrolysis of organonitrate functional groups in aerosol particles, *Aerosol Sci. Technol.*, *46*(12), 1359–1369, doi:10.1080/02786826.2012.716175.

Meng, J. W., M. C. Yeung, Y. J. Li, B. Y. L. Lee, and C. K. Chan (2014), Size-resolved cloud condensation nuclei (CCN) activity and closure analysis at the HKUST Supersite in Hong Kong, *Atmos. Chem. Phys.*, *14*(18), 10,267–10,282, doi:10.5194/acp-14-10267-2014.

Middlebrook, A. M., R. Bahreini, J. L. Jimenez, and M. R. Canagaratna (2012), Evaluation of composition-dependent collection efficiencies for the aerodyne aerosol mass spectrometer using field data, *Aerosol Sci. Technol.*, *46*(3), 258–271, doi:10.1080/02786826.2011.620041.

Mohr, C., J. A. Huffman, M. J. Cubison, A. C. Aiken, K. S. Docherty, J. R. Kimmel, I. M. Ulbrich, M. Hannigan, and J. L. Jimenez (2009), Characterization of primary organic aerosol emissions from meat cooking, trash burning, and motor vehicles with high-resolution aerosol mass spectrometry and comparison with ambient and chamber observations, *Environ. Sci. Technol.*, *43*(7), 2443–2449, doi:10.1021/es8011518.

National Ambient Air Quality Standards (NAAQS) (2012), *National Ambient Air Quality Status and Trends in India-2010*, *Cent. Pollut. Control Board*, Ministry of Environment and Forests, New Delhi.

Ng, N. L., et al. (2010), Organic aerosol components observed in Northern Hemispheric datasets from aerosol mass spectrometry, *Atmos. Chem. Phys.*, *10*(10), 4625–4641, doi:10.5194/acp-10-4625-2010.

Ng, N. L., M. R. Canagaratna, J. L. Jimenez, P. S. Chhabra, J. H. Seinfeld, and D. R. Worsnop (2011), Changes in organic aerosol composition with aging inferred from aerosol mass spectra, *Atmos. Chem. Phys.*, *11*(13), 6465–6474, doi:10.5194/acp-11-6465-2011.

Ortega, A. M., D. A. Day, M. J. Cubison, W. H. Brune, D. Bon, J. A. de Gouw, and J. L. Jimenez (2013), Secondary organic aerosol formation and primary organic aerosol oxidation from biomass-burning smoke in a flow reactor during FLAME-3, *Atmos. Chem. Phys.*, *13*(22), 11,551–11,571, doi:10.5194/acp-13-11551-2013.

Osto, M. D., R. M. Harrison, H. Coe, and P. Williams (2009), Real-time secondary aerosol formation during a fog event in London, *Atmos. Chem. Phys.*, *9*, 2459–2469.

Paatero, P., and U. Tapper (1994), Positive matrix factorization—A nonnegative factor model with optimal utilization of error estimates of data values, *Environmetrics*, *5*, 111–126, doi:10.1002/env.3170050203.

Patidar, V., S. N. Tripathi, P. K. Bharti, and T. Gupta (2012), First surface measurement of cloud condensation nuclei over Kanpur, IGP: Role of long range transport, *Aerosol Sci. Technol.*, *46*, 973–982, doi:10.1080/02786826.2012.685113.

Quan, J., Q. Zhang, H. He, J. Liu, M. Huang, and H. Jin (2011), Analysis of the formation of fog and haze in North China Plain (NCP), *Atmos. Chem. Phys.*, *11*(15), 8205–8214, doi:10.5194/acp-11-8205-2011.

Ram, K., and M. M. Sarin (2011), Day-night variability of EC, OC, WSOC and inorganic ions in urban environment of Indo-Gangetic Plain: Implications to secondary aerosol formation, *Atmos. Environ.*, *45*(2), 460–468, doi:10.1016/j.atmosenv.2010.09.055.

Ram, K., M. M. Sarin, and S. N. Tripathi (2012), Temporal trends in atmospheric PM2.5, PM10, elemental carbon, organic carbon, water-soluble organic carbon, and optical properties: Impact of biomass burning emissions in the Indo-Gangetic Plain, *Environ. Sci. Technol.*, *46*(2), 686–695, doi:10.1021/es202857w.

Ryu, S. Y., B. G. Kwon, Y. J. Kim, H. H. Kim, and K. J. Chun (2007), Characteristics of biomass burning aerosol and its impact on regional air quality in the summer of 2003 at Gwangju, Korea, *Atmos. Res.*, *84*, 362–373, doi:10.1016/j.atmosres.2006.09.007.

Saarikoski, S. K., M. K. Sillanpaeae, K. M. Saarnio, R. E. Hillamo, A. S. Pennanen, and R. O. Salonen (2008), Impact of biomass combustion on urban fine particulate matter in Central and Northern Europe, *Water Air Soil Pollut.*, *191*(1–4), 265–277, doi:10.1007/s11270-008-9623-1.

Sarkar, S., P. S. Khillare, D. S. Jyethi, A. Hasan, and M. Parween (2010), Chemical speciation of respirable suspended particulate matter during a major firework festival in India, *J. Hazard. Mater.*, *184*(1–3), 321–330, doi:10.1016/j.jhazmat.2010.08.039.

Seinfeld, J. H., and J. F. Pankow (2003), Organic atmospheric particulate material, *Annu. Rev. Phys. Chem.*, *54*, 121–140, doi:10.1146/annurev.physchem.54.011002.103756.

Seinfeld, J. H., and S. N. Pandis (2006), *Atmospheric Chemistry and Physics: From Air Pollution to Climate Change*, 2nd ed., John Wiley, New York.

Shilling, J. E., et al. (2009), Loading-dependent elemental composition of α-pinene SOA particles, *Atmos. Chem. Phys.*, *9*(3), 771–782.

Singh, D. K., Lakshay, and T. Gupta (2014), Field performance evaluation during fog-dominated wintertime of a newly developed denuder-equipped PM1 sampler, *Environ. Sci. Pollut. Res.*, *21*(6), 4551–4564, doi:10.1007/s11356-013-2371-9.

Singh, V. P. (2011), Experimental study of the effects of environmental and fog condensation nuclei parameters on the rate of fog formation and dissipation using a new laboratory scale fog generation facility, *Aerosol Air Qual. Res.*, *11*, 140–154, doi:10.4209/aaqr.2010.08.0071.

Takegawa, N., T. Miyakawa, K. Kawamura, and Y. Kondo (2007), Contribution of selected dicarboxylic and omega-oxocarboxylic acids in ambient aerosol to the m/z 44 signal of an aerodyne aerosol mass spectrometer, *Aerosol Sci. Technol.*, *41*(4), 418–437, doi:10.1080/02786820701203215.

Tare, V., et al. (2006), Measurements of atmospheric parameters during Indian Space Research Organization Geosphere Biosphere Program Land Campaign II at a typical location in the Ganga Basin: 2. Chemical properties, *J. Geophys. Res.*, *111*, D23210, doi:10.1029/2006JD007279.

Timonen, H., et al. (2013), Characteristics, sources and water-solubility of ambient submicron organic aerosol in springtime in Helsinki, Finland, *J. Aerosol Sci.*, *56*, 61–77, doi:10.1016/j.jaerosci.2012.06.005.

Ulbrich, I. M., M. R. Canagaratna, Q. Zhang, D. R. Worsnop, and J. L. Jimenez (2009), Interpretation of organic components from positive matrix factorization of aerosol mass spectrometric data, *Atmos. Chem. Phys.*, *9*(9), 2891–2918.

Venkataraman, C., C. K. Reddy, S. Josson, and M. S. Reddy (2002), Aerosol size and chemical characteristics at Mumbai, India, during the INDOEX-IFP (1999), *Atmos. Environ.*, *36*(12), 1979–1991, doi:10.1016/s1352-2310(02)00167-x.

Wood, E. C., et al. (2010), Investigation of the correlation between odd oxygen and secondary organic aerosol in Mexico City and Houston, *Atmos. Chem. Phys.*, *10*(18), 8947–8968, doi:10.5194/acp-10-8947-2010.

Zhang, J. K., Y. Sun, Z. R. Liu, D. S. Ji, B. Hu, Q. Liu, and Y. S. Wang (2014), Characterization of submicron aerosols during a month of serious pollution in Beijing, 2013, *Atmos. Chem. Phys.*, *14*(6), 2887–2903, doi:10.5194/acp-14-2887-2014.

Zhang, Q., M. R. Canagaratna, J. T. Jayne, D. R. Worsnop, and J. L. Jimenez (2005), Time- and size-resolved chemical composition of submicron particles in Pittsburgh: Implications for aerosol sources and processes, *J. Geophys. Res.*, *110*, D07S09, doi:10.1029/2004JD004649.

Zhang, Q., J. L. Jimenez, D. R. Worsnop, and M. Canagaratna (2007a), A case study of urban particle acidity and its influence on secondary organic aerosol, *Environ. Sci. Technol.*, *41*(9), 3213–3219, doi:10.1021/es061812j.

Zhang, Q., et al. (2007b), Ubiquity and dominance of oxygenated species in organic aerosols in anthropogenically-influenced Northern Hemisphere midlatitudes, *Geophys. Res. Lett.*, *34*, L13801, doi:10.1029/2007GL029979.

Zhang, Y. J., et al. (2015), Insights into characteristics, sources, and evolution of submicron aerosols during harvest seasons in the Yangtze River delta region, China, *Atmos. Chem. Phys.*, *15*(3), 1331–1349, doi:10.5194/acp-15-1331-2015.